Available online at www.sciencedirect.com

ScienceDirect

Solar Energy 107 (2014) 660–667

SOLAR ENERGY

www.elsevier.com/locate/solener

Multiwalled carbon nanotube thin films prepared by aerosol deposition process for use as highly efficient Pt-free counter electrodes of dye-sensitized solar cells

Ji Young Ahn [a], Ji Hoon Kim [a], Jong Man Kim [a], Donggeun Lee [b], Soo Hyung Kim [a,*]

[a] Department of Nanofusion Technology, Pusan National University, 30 Jangjeon-dong, Geumjung-gu, Busan 609-735, Republic of Korea
[b] School of Mechanical Engineering, Pusan National University, 30 Jangjeon-dong, Geumjung-gu, Busan 609-735, Republic of Korea

Received 6 February 2014; received in revised form 7 June 2014; accepted 11 June 2014

Communicated by: Associate Editor Frank Nuesch

Abstract

In this study, transparent and catalytic multiwalled carbon nanotube (MWCNT) thin films with controlled thickness were fabricated using a simple and conventional multiple nozzle-based aerosol deposition process (ADP). MWCNTs were homogeneously dispersed in deionized water via surfactant treatment, and the MWCNT-dispersed aqueous solution was then aerosolized and deposited on fluorine-doped tin oxide glass substrates to form MWCNT thin films. The characteristics of MWCNTs, degree of MWCNT dispersion stability in the aqueous solution, and morphology and light transmittance of the prepared MWCNT thin films were systematically examined. Finally, the prepared MWCNT thin films were used as the counter electrodes (CEs) of dye-sensitized solar cells (DSSCs). For comparison purposes, the photovoltaic performance of DSSCs composed of MWCNT thin-film CEs was compared to that of reference DSSCs composed of conventional Pt thin-film CEs. The results showed that the power conversion efficiency of DSSCs composed of critical amount of MWCNTs coated on CEs was almost equal or slightly higher than that of conventional Pt-based DSSCs. Thus, it can be concluded that the ADP-assisted precisely controlled accumulation of transparent and catalytic MWCNT thin films on the CEs of DSSCs is a very promising approach for replacing the expensive Pt metal that is currently used in DSSC industries.

Keywords: Multiwalled carbon nanotubes; Aerosol deposition process; Dye-sensitized solar cells; Counter electrodes

1. Introduction

Dye-sensitized solar cells (DSSCs) have been developed extensively because of the relatively low cost involved in their manufacturing processes (Grätzel, 2001, 2003; O'Regan and Grätzel, 1991). Among the various components of DSSCs, the counter electrode (CE) is one of the most important parts because it collects the photogenerated electrons from an external circuit and simultaneously regenerates dye sensitizers by reducing the iodide electrolyte used (Halme et al., 2006; Murakami and Grätzel, 2008; Papageorgiou, 2004). In order to fabricate CEs for DSSCs, Pt is generally coated on the surface of fluorine-doped tin oxide (FTO) glass substrates because Pt has high electrochemical reactivity (Fang et al., 2004; Lin et al., 2010; Olsen et al., 2000). However, since Pt is a relatively expensive noble metal and dissolves slowly in corrosive iodide electrolytes, it is necessary to find an appropriate replacement of Pt as a comparable potential catalytic material for DSSCs. Furthermore, the CEs of DSSCs should be stable and transparent for various applications such as

* Corresponding author. Tel.: +82 519307737.
E-mail address: sookim@pusan.ac.kr (S.H. Kim).

http://dx.doi.org/10.1016/j.solener.2014.06.015
0038-092X/

building-integrated photovoltaic cells (Heiniger et al., 2013; Jelle et al., 2012; Yoon et al., 2011) and tandem cells (Ahn et al., 2007; Dürr et al., 2004; Nattestad et al., 2008), as well as simultaneously have low electrical resistance and high electrocatalytic reactivity for effectively reducing iodide/tri-iodide (I^-/I_3^-) electrolytes.

In addition to being inexpensive, multiwalled carbon nanotubes (MWCNTs) have rapid electron transfer kinetics, a relatively large specific surface area, and high electrocatalytic activity; therefore, numerous research groups have employed MWCNTs as a replacement of Pt for fabricating the CEs of DSSCs (Anwar et al., 2013; Cha et al., 2010; Hsieh et al., 2011; Lee et al., 2009, 2010; Yan et al, 2013). Typically, MWCNTs are coated on FTO glass to be used as a CE for DSSCs. In order to fabricate MWCNT-coated FTO glass CEs, various techniques such as doctor blade (Cha et al., 2010; Hsieh et al., 2011; Lee et al., 2009; Li et al., 2010), screen printing (Anwar et al., 2013), spin coating (Fan et al., 2008; Jo et al., 2012), spray coating processes (Hsieh et al., 2011; Huang et al., 2012; Ramasamy et al., 2008), and hydrothermal deposition (Siriroj et al., 2012) have been developed. However, these techniques suffer from some inherent problems in fabricating uniform MWCNT layers with precisely controlled thickness owing to the formation of highly agglomerated and entangled MWCNTs during the aforementioned coating processes. Forming a non-uniform MWCNT thin film on an FTO glass substrate as a CE can eventually deteriorate electron transfer in DSSCs. Therefore, a more versatile and reliable method is required to realize a uniform spatial distribution of MWCNTs on an FTO glass substrate for use in DSSCs.

In this study, we developed a multiple nozzle-based aerosol deposition process (ADP) for a MWCNT-dispersed aqueous solution, and subsequently employed the process for fabricating MWCNT-deposited thin films on FTO glass substrates for assembling CEs of DSSCs. Further, we systematically investigated the effect of fabricated MWCNT thin films on the photovoltaic performance of the resulting DSSCs. Various DSSCs containing MWCNT-deposited CEs were then compared with conventional DSSCs containing Pt-deposited CEs.

2. Experimental

2.1. Fabrication of MWCNT-dispersed aqueous solution

First, MWCNTs were purchased from CNT Co., Ltd (Korea) and used without further treatment. The MWCNTs were generated using a thermal CVD method, and they had the average diameter of ~20 nm and the length distribution of 1–25 μm. The purity of MWCNTs was larger than approximately 95% and the specific surface area was approximately 150–250 m^2/g. In order to prepare a homogeneously MWCNT-dispersed aqueous solution, the surfactant addition method was employed. Appropriate surfactant addition can homogeneously disperse inherently hydrophobic MWCNTs in an aqueous solution by forming an interconnection between hydrophilic and hydrophobic surfaces. In the surfactant addition method, carboxy methyl cellulose (CMC, Sigma Aldrich, Mw: 700,000) was used as the surfactant (Cha et al., 2010; Imoto et al., 2003; Lee et al., 2009; Takahashi et al., 2006). CMC is a kind of surfactant with several hydroxyl groups, and it has good properties of stabilizing the stock, implying that the long CMC molecules wrap around the MWCNTs and allowing them to be homogeneously dispersed in water. A CMC-added MWCNT aqueous solution containing 0.1 wt% of MWCNTs and 0.15 wt% of CMC in deionized water was prepared by sonicating the solution for 1 h.

2.2. Aerosol deposition process (ADP) for preparing MWCNT-dispersed aqueous solution

MWCNT-deposited CEs were fabricated by depositing the aerosolized MWCNTs onto FTO glass substrates as shown in Fig. 1. The ADP system used for this approach

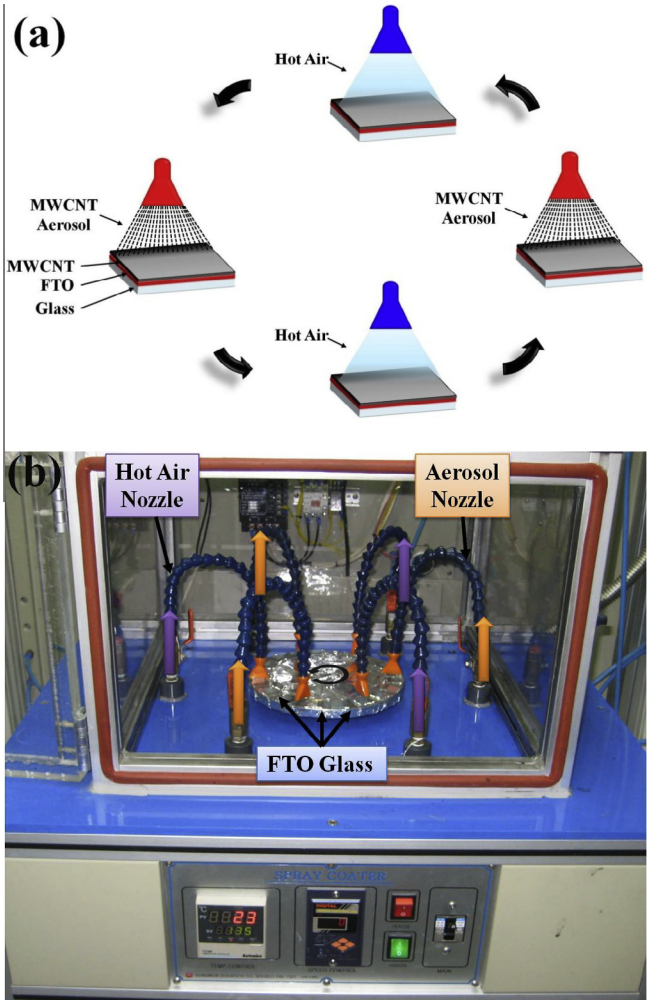

Fig. 1. (a) Schematic and (b) photograph of an aerosol deposition process system for fabricating MWCNT thin films on FTO glass substrates.

consisted of multiple aerosol nozzles, hot air nozzles, and a rotating plate. An external vacuum filter system was used for removing the excess amount of MWCNT aerosol. The MWCNT aerosol generated by an atomizer operated by filtered compressed air at 35 psi was injected through the multiple aerosol nozzles, and MWCNT thin films were then continuously formed on the FTO glass substrates, which were placed on the rotating plate with a rotation speed of 1 rpm. In the meantime, the formed MWCNT thin films were rapidly dried by hot air (~120 °C), which was injected through the multiple hot air nozzles.

2.3. Characterization of MWCNT aqueous solution and thin films

The morphology of MWCNTs and MWCNT-deposited thin films was characterized by scanning electron microscopy (SEM; Hitachi, Ltd., S-4200) operated at ~15 kV and transmission electron microscopy (TEM; JEOL, JEM-2010) operated at ~200 kV. UV–Vis NIR spectroscopy (Varian Inc., Cary 500) was carried out to quantify the dispersion stability of the MWCNT aqueous solution; the absorbance of the solution at a wavelength of ~550 nm was measured (Moon et al., 2009).

2.4. Fabrication and photovoltaic property characterization of DSSCs

Commercially available titanium dioxide nanoparticles (TiO_2 NPs; P25, Degussa) were used without further treatment to form a photocatalytic active layer, which was screen-printed on FTO glass (SnO_2:F, 7 Ω/sq, Pilkington) with an active area of $0.6 \times 0.6\ cm^2$ and an average thickness of approximately 20 μm. The TiO_2 NPs were the mixture of anatase and rutile phases, and they had the average diameter of approximately 25 nm and the specific surface area of approximately $50\ m^2/g$. To prepare TiO_2 paste for the screen-printing process, 6 g of TiO_2 NPs, 15 g of ethanol, 1 mL of acetic acid (CH_3COOH), and 20 g of terpineol were mixed in a vial and sonicated for 1 h. Simultaneously, a solution containing 3 g of ethylcellulose dissolved in 27 g of ethanol was also prepared. Subsequently, the two solutions were mixed in a vial for 5 min by using a planetary mixer. The resulting TiO_2-NP-accumulated layer formed on FTO glass via the screen-printing process was then sintered in an electric furnace at 500 °C for 30 min. The sintered layer was subsequently immersed in anhydrous ethanol containing 0.3 mM of the Ru-dye $(Bu_4N)_2[Ru(Hdcbpy)_2\text{-}(NCS)_2]$ (N719 dye, Solaronix) for 24 h at room temperature in order to allow the dye molecules to attach themselves to the entire surface of the TiO_2 NPs. The dye-adsorbed TiO_2-NP-based photoelectrode was then rinsed with ethanol and dried in a convection oven at 80 °C for 10 min. As a reference counter electrode, Pt-coated FTO glass was also prepared via ion sputtering (model No. E1010, Hitachi) carried out at 2.5 kV. Both the photoelectrode (i.e., TiO_2-coated FTO glass) and counter electrode (i.e., Pt- and MWCNT-coated FTO glasses) were then sealed together with a hot-melt polymer film (60 μm thickness, Surlyn, DuPont) inserted between them. Moreover, an iodide-based liquid electrolyte (AN-50, Solaronix) was injected into the interspace between the electrodes.

The current density–voltage (J–V) characteristics of the resulting DSSCs fabricated using this approach were measured under AM 1.5 simulated illumination with an intensity of $100\ mW/cm^2$ (PEC-L11, Peccell Technologies, Inc.). The intensity of sunlight illumination was calibrated using a standard Si photodiode detector with a KG-5 filter. The J–V curves were automatically recorded using a Keithley SMU 2400 source meter by illuminating the DSSCs. The photovoltaic properties of DSSCs were characterized using the solar simulator (PEC-L11, Peccell Technologies, Inc.) based on following Eqs. (1)–(4). The final power conversion efficiency (PCE) was determined by the open circuit voltage (V_{oc}), the short circuit current density (J_{sc}), the fill factor (FF) and the incident light intensity.

$$I_{SC} = \int qF(\lambda)(1 - r(\lambda))IPCE(\lambda)d\lambda \tag{1}$$

$$V_{OC} = \frac{kT}{q} \ln\left(\frac{I_{inj}}{I_O} + 1\right) \tag{2}$$

$$FF = \frac{J_m V_m}{J_{SC} V_{OC}} \tag{3}$$

$$PCE = \frac{J_m V_m}{P_{in}} = \frac{FF(J_{SC} V_{OC})}{P_{in}} \tag{4}$$

where q is the electron charge, λ is the wavelength, $F(\lambda)$ is the incident photon flux density, $r(\lambda)$ is the incident light loss in light absorption and reflection by the conducting glass, $IPCE(\lambda)$ is the incident photon-to-electron conversion efficiency of cell over the λ of the incident light, k is the Boltzmann constant, T is the absolute temperature, q is the magnitude of the electron charge, I_{inj} is the concentration of electrons injected to the TiO_2, I_o is the dark current (i.e., $I_o = qn_o k_{et}[I_3^-]$, where n_o is the electron density of the conduction band of the TiO_2 in the dark, k_{et} is the rate constant for recombination, and $[I_3^-]$ is the concentration of the oxidized redox mediator in the liquid electrolyte.), J_m is the maximum current density, V_m is the maximum voltage, and P_{in} is the incident light intensity.

3. Results and discussion

We first prepared a MWCNT-dispersed aqueous solution prior to the aerosolization of MWCNTs. In order to increase the dispersion stability of MWCNTs, CMC was added to the MWCNT-dispersed aqueous solution as a surfactant. After the preparation of this CMC-treated MWCNT aqueous solution, a series of UV–Vis spectroscopic measurements were carried out to quantify the dispersion stability of MWCNTs in the aqueous solution, as shown in Fig. 2. Here, the dispersion stability of MWCNTs

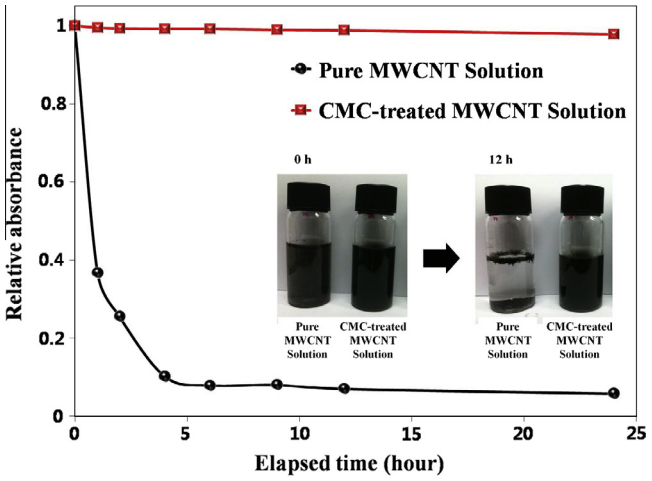

Fig. 2. Dispersion stability of an MWCNT aqueous solution with and without CMC-based surfactant treatment as measured by UV–Vis spectroscopy.

in the aqueous solution was evaluated by calculating the relative absorbance as the ratio of the absorbance of MWCNTs at the initial time to the absorbance of MWCNTs after each elapsed time period at a wavelength of 550 nm. It was found that the relative absorbance of MWCNTs dispersed in the aqueous solution without any surfactant treatment significantly decreased with time. However, the relative absorbance of the CMC-treated MWCNT aqueous solution did not show any considerable change with elapsed time. This suggests that the CMC-treated MWCNT solution had relatively much higher long-term dispersion stability owing to reduction in the degree of agglomeration of the MWCNTs dispersed in the aqueous solution. Thus, untangled and homogeneous MWCNT aerosols can be generated by atomizing the CMC-treated MWCNT solution in the ADP system.

The as-received MWCNTs were inherently bent and bundled, as shown in SEM and TEM images (see Fig. 3a and b). They were composed of up to ~20 walls and a

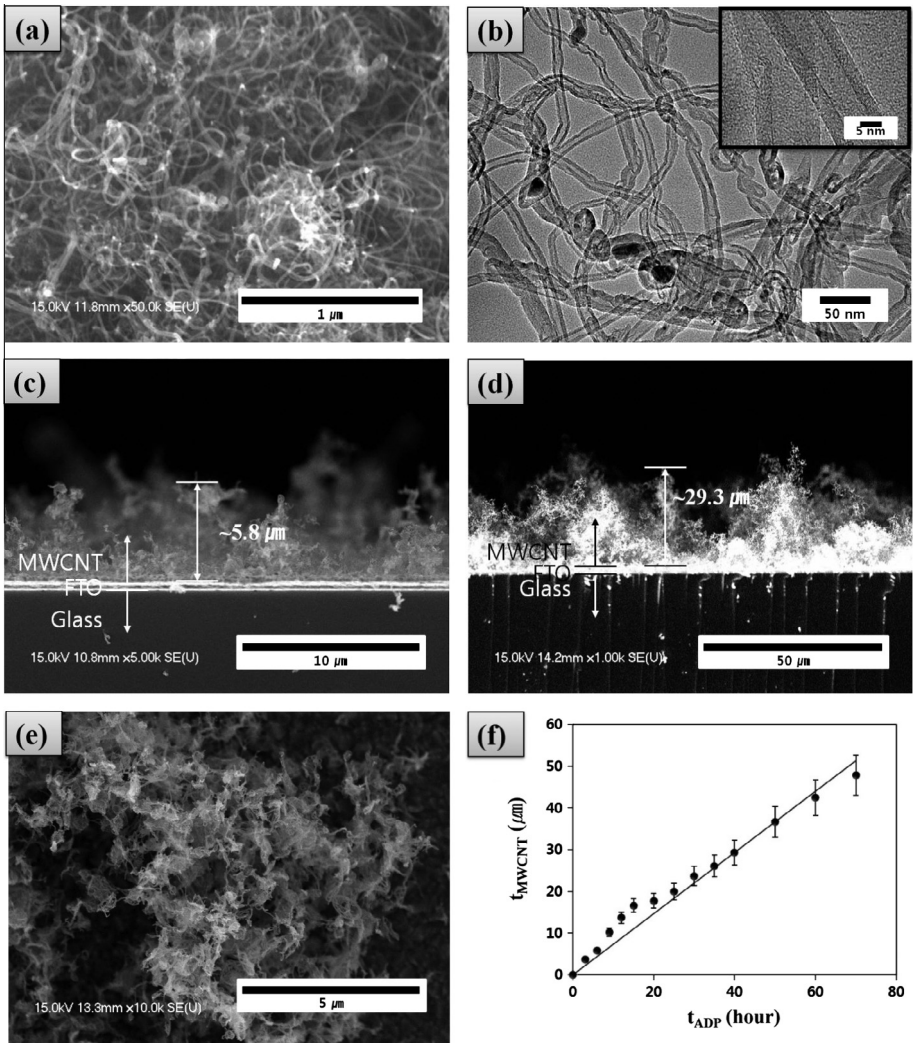

Fig. 3. (a) SEM and (b) TEM images of MWCNTs (the inset shows an HRTEM image of MWCNTs). Side-view SEM images of MWCNT thin films deposited for (c) 6 h and (d) 40 h. (e) Top-view SEM image of MWCNT thin film deposited for 40 h on the FTO glass. (f) Increase in MWCNT thin film thickness as a function of ADP time.

hollow core with an outer diameter of ~20 nm (see the inset of Fig. 3b). At the short ADP times of less than 2–3 h, the uniformity of MWCNT thin film was found to be very poor. However, the longer ADP time resulted in a much more homogeneous deposition of MWCNTs on the FTO glass substrate by MWCNT interconnection due to repeated liquid densification process. This suggests that the uniformity of MWCNT thin films is enhanced with increasing ADP time of MWCNTs as shown in Fig. 3c–e.

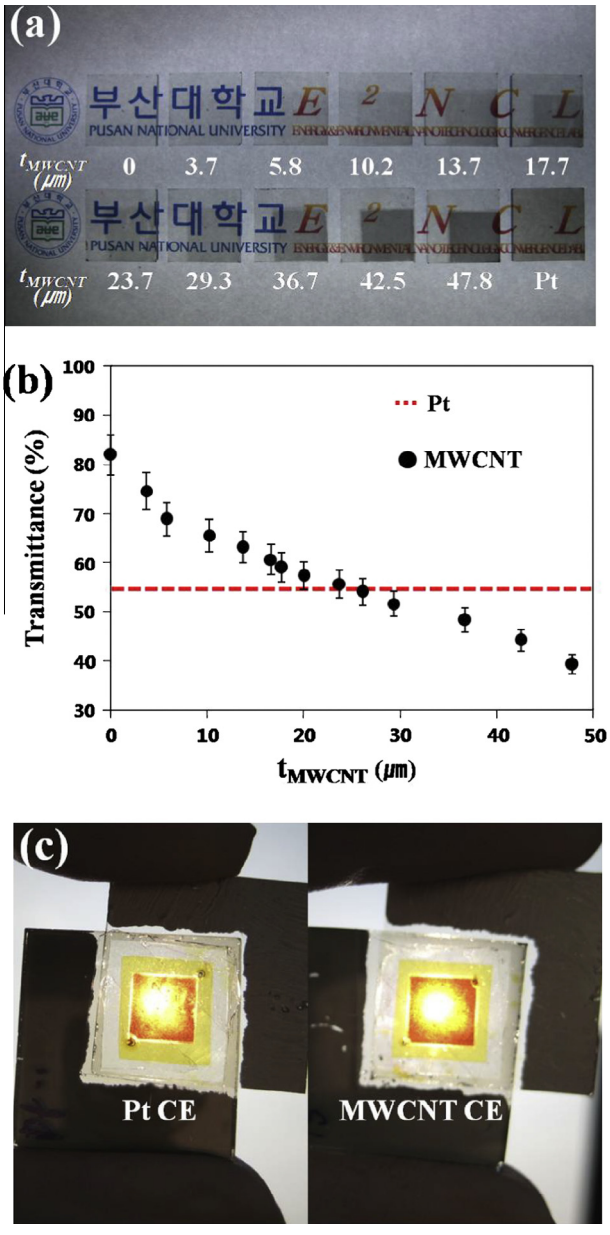

Fig. 4. (a) Photographs of MWCNT-coated FTO glass substrates prepared by varying the MWCNT thin film thickness, (b) changes in light transmittance of MWCNT thin films as a function of the MWCNT thin film thickness (the red dotted line denotes reference transmittance for a Pt-coated FTO glass substrate), and (c) photographs of DSSCs assembled with Pt- and MWCNT (t_{MWCNT} = ~48 μm)-deposited counter electrodes. (For interpretation of the references to color in this figure legend, the reader is referred to the web version of this article.)

The thickness of a typical MWCNT thin film formed on the FTO glass substrate was found to increase linearly from ~5.8 μm for 6 h ADP to ~29.3 μm for 40 h ADP, as shown in Fig. 3c and d, respectively. The average thickness of the formed MWCNT thin films increased linearly with increasing ADP time, and the average thickness increase rate of the MWCNT thin films formed via this approach was calculated to be ~0.75 ± 0.15 μm/h, as shown in Fig. 3f.

The transparency of MWCNT-deposited FTO glass decreased qualitatively with increasing thickness of the MWCNT thin film, as shown in Fig. 4a. This suggests that the transparency and thickness of MWCNT thin films formed on FTO glass can be easily controlled by varying the ADP time. The light transmittance of MWCNT thin films formed on FTO glass substrates was quantitatively measured using UV–Vis spectroscopy, and the obtained results were then compared with those for a typical Pt thin film coated on a FTO glass substrate via ion-beam sputtering, as shown in Fig. 4b. Here, the light transmittance was determined at a wavelength of ~550 nm. The light transmittance of FTO glass was observed to be ~82%, and that of MWCNT-deposited FTO glass ranged from 40% to 75%. Further, the light transmittance of the reference Pt-deposited FTO glass was found to be ~55%. On the basis of the positive results obtained for ADP-assisted MWCNT thin films, various Pt-free transparent MWCNT-deposited FTO glasses were employed as CEs for DSSCs. As shown in Fig. 4c, the transparencies of DSSCs with Pt- and MWCNT (t_{MWCNT} = ~48 μm)-deposited CEs assembled using the proposed approach did not show any significant difference. This observation suggests that MWCNTs can be a promising material for fabricating the CEs of DSSCs as their transparency is comparable to that of Pt.

The effects of various MWCNT thin films—used as a catalytic conducting material for fabricating CEs—on the photovoltaic performance of DSSCs were systematically examined by observing current density–voltage (*J–V*)

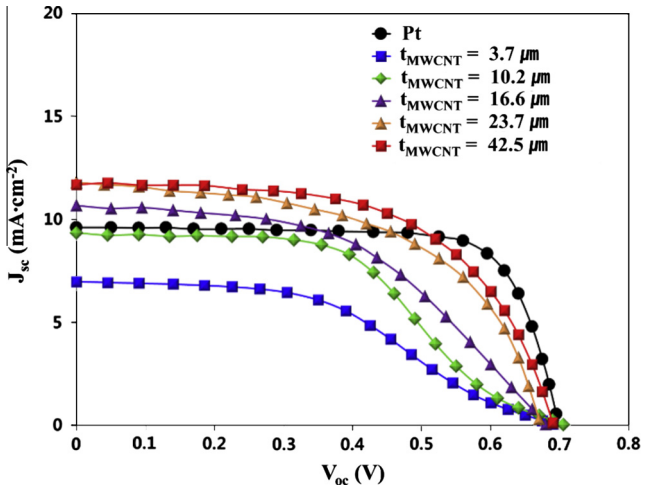

Fig. 5. Current density–voltage (*J–V*) curves for DSSCs containing Pt- and MWCNT thin film-coated counter electrode.

curves as shown in Fig. 5. The photovoltaic performance of DSSCs containing MWCNT CEs was then compared to a reference DSSC containing a Pt-deposited CE as shown in Fig. 6. Here, other parameters such as the TiO_2 layer, organic dye, and liquid electrolyte were fixed for making a direct comparison. Table 1, Figs. 5 and 6 show that both short circuit current density (J_{sc}) and fill factor (FF) increased significantly upon increasing the MWCNT thin film thickness up to ~20 μm. Subsequently, J_{sc} and FF appeared to be stabilized with further increase in the MWCNT thin film thickness up to ~48 μm, as shown in Fig. 6a and c. However, the open circuit voltage (V_{oc}) did not change significantly upon increasing the MWCNT thin film thickness, as shown in Fig. 6b. The resulting power conversion efficiency (PCE) of DSSCs with MWCNT CEs increased with increasing MWCNT thin film thickness, and then saturated to that of the DSSC with a Pt CE, as shown in Fig. 6d. Using the proposed approach, the maximum values of the DSSC photovoltaic properties were found to be V_{oc}: ~0.68 V, J_{sc}: ~12.69 mA/cm^2, FF: ~0.60, and PCE: ~5.18% for the case of CE with a MWCNT thin film thickness of 60–70 μm. For comparison, the photovoltaic properties of the DSSC with a conventional Pt CE were V_{oc}: ~0.70 V, J_{sc}: ~9.57 mA/cm^2,

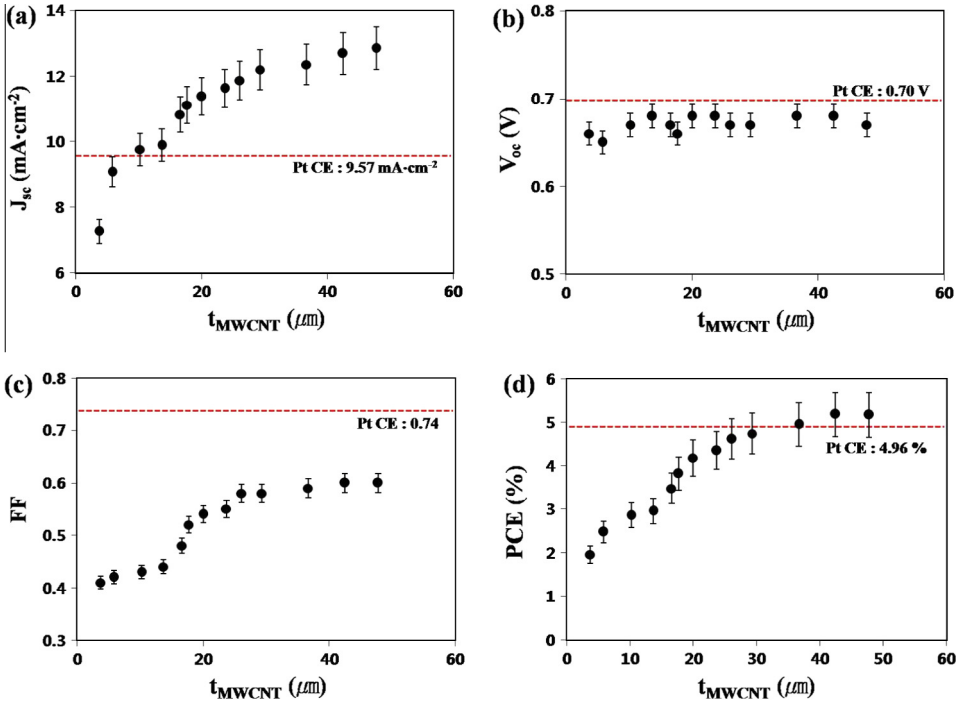

Fig. 6. Changes in photovoltaic performance ((a) J_{sc}, (b) V_{oc}, (c) FF, and (d) PCE) of DSSCs by varying the MWCNT thin-film thickness.

Table 1
Summary of photovoltaic characteristics of various DSSCs with Pt- and MWCNT-coated counter electrodes.

Counter electrode	t_{ADP} (h)	t_{MWCNT} (μm)	J_{sc} (mA/cm^2)	V_{oc} (V)	FF	PCE (%)	τ_e (ms)	R_l (Ω)	R_{rec} (Ω)	R_{ct} (Ω)
Pt	–	–	9.57 ± 0.18	0.70 ± 0.01	0.74 ± 0.01	4.96 ± 0.10	5.0	2	9	7
	3	3.7	7.26 ± 0.08	0.66 ± 0.01	0.41 ± 0.01	1.96 ± 0.07	0.4	0.2	371	52
	6	5.8	9.08 ± 0.03	0.65 ± 0.01	0.42 ± 0.01	2.48 ± 0.08	0.4	0.3	282	46
	9	10.2	9.76 ± 0.20	0.67 ± 0.01	0.43 ± 0.02	2.86 ± 0.13	0.5	0.5	79	39
	12	13.7	9.89 ± 0.21	0.68 ± 0.01	0.44 ± 0.01	2.96 ± 0.07	1.1	0.8	66	28
	15	16.6	10.83 ± 0.22	0.67 ± 0.01	0.48 ± 0.01	3.48 ± 0.08	1.7	1.0	35	23
	20	17.7	11.12 ± 0.19	0.66 ± 0.01	0.52 ± 0.01	3.82 ± 0.20	2.0	2.0	28	13
MWCNT	25	20.0	11.38 ± 0.13	0.68 ± 0.01	0.54 ± 0.01	4.18 ± 0.11	2.6	3.0	23	11
	30	23.7	11.63 ± 0.25	0.68 ± 0.01	0.55 ± 0.02	4.35 ± 0.19	3.1	4.0	18	10
	35	26.1	11.87 ± 0.11	0.67 ± 0.01	0.58 ± 0.01	4.61 ± 0.16	4.3	4.4	16	9
	40	29.3	12.20 ± 0.31	0.67 ± 0.01	0.58 ± 0.02	4.74 ± 0.27	5.0	4.8	11	8
	50	36.7	12.35 ± 0.09	0.68 ± 0.01	0.59 ± 0.01	4.95 ± 0.22	5.1	5.5	10	7
	60	42.5	12.69 ± 0.35	0.68 ± 0.01	0.60 ± 0.01	5.18 ± 0.17	5.4	6.2	8	6
	70	47.8	12.85 ± 0.22	0.67 ± 0.01	0.60 ± 0.01	5.17 ± 0.17	5.5	7.4	7	5

Note: Aerosol deposition process (ADP) time (t_{ADP}), MWCNT thin-film thickness (t_{MWCNT}), short circuit current (J_{sc}), open circuit voltage (V_{oc}), fill factor (FF), power conversion efficiency (PCE), electron lifetime (τ_e), Pt or MWCNT layer resistance (R_l), recombination resistance (R_{rec}), charge transfer resistance (R_{ct}).

FF: ~0.74, and *PCE*: ~4.96%. These results suggest that MWCNTs can be a promising replacement of Pt because (1) the catalytic reaction at the CE in DSSCs effectively occurs on MWCNTs, and (2) increasing the thickness of a MWCNT thin film on the CE enhances the photovoltaic performance of DSSCs. This is because more accumulation of MWCNTs on CEs increased the interfacial contact area between MWCNTs and the liquid electrolyte. This in turn resulted in faster completion of I_3^- reduction and decrease in charge transfer resistance owing to rapid electron transport through the MWCNT medium with relatively high electrical conductivity.

The above-mentioned result was corroborated by an electrochemical impedance spectroscopy (EIS) analysis, as shown in Table 1 and Fig. 7. Nyquist plots (Fig. 7a) clearly show that an increase in the MWCNT thin-film thickness significantly reduced the charge transfer resistance (R_{ct}) at the TiO_2, dye, electrolyte, and CE interfaces. Simultaneously, the MWCNT layer resistance (R_l) was observed to be slightly increased. However, the changed values of R_l were negligibly small compared to those of R_{ct}, implying that the effective and fast charge transfer predominantly promotes the photovoltaic performance of DSSCs containing MWCNT thin films in CEs. Fig. 7b shows Bode phase plots for analyzing the electron lifetime. The maximum frequency shifted to a lower value with an increase in the thickness of the MWCNT thin film on the CE, and the electron lifetime ($\tau_e = [2\pi f_{max}]^{-1}$, where f_{max} is the maximum frequency) increased from 0.4 ms ($t_{MWCNT} = \sim 3.7$ μm) to 5.5 ms ($t_{MWCNT} = \sim 47.8$ μm). This result suggests that photogenerated electrons could diffuse through TiO_2-coated photoelectrodes and MWCNT-coated CEs when their direct recombination with dyes and electrolytes was reduced, which occurred inherently upon increasing the amount of MWCNTs on CEs.

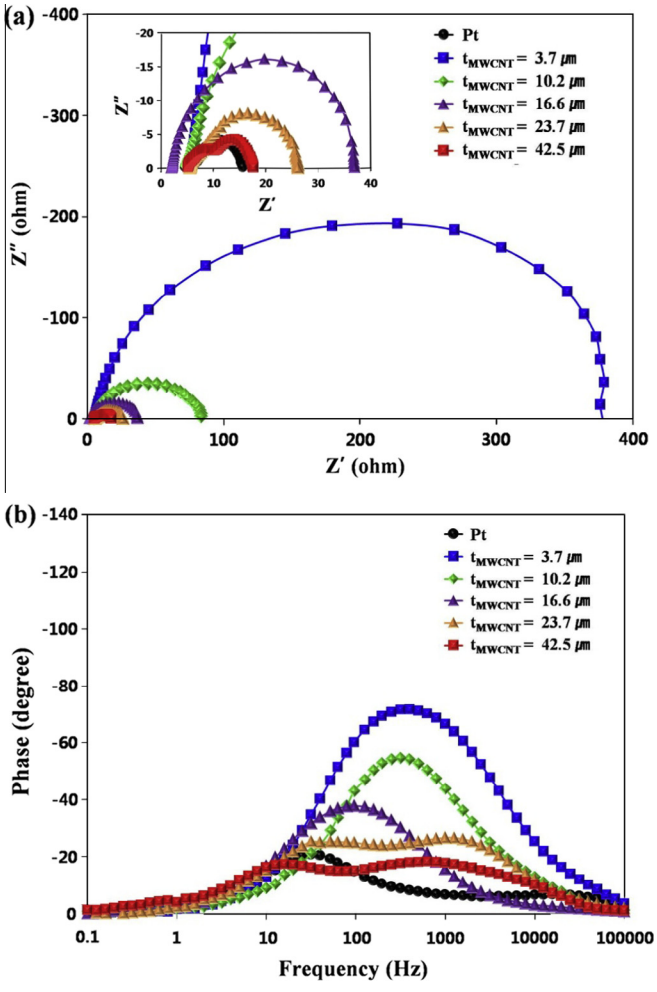

Fig. 7. (a) Nyquist plots and (b) Bode plots for DSSCs containing Pt- and MWCNT-coated counter electrodes.

4. Conclusions

We have fabricated ADP-assisted MWCNT thin films on CEs to examine the effects of these films on the photovoltaic performance of DSSCs. By varying the ADP time, the MWCNT thin film thickness was precisely controlled with an average increase rate of ~0.75 ± 0.15 μm/h. Further, the resulting MWCNT thin film-based CEs were observed to be transparent with light transmittance ranging from ~80% (without MWCNTs) to ~40% (with an MWCNT thin film of ~48 μm thickness). After assembling DSSCs containing various MWCNT thin films on CEs, their photovoltaic performance was compared to that of a reference DSSC containing a Pt CE. The results showed that J_{sc}, *FF*, and *PCE* of DSSCs with MWCNT CEs increased significantly upon increasing the MWCNT thin film thickness owing to an increase in the catalytic surface area at the MWCNT and electrolyte interface and a simultaneous decrease in the charge transfer resistance due to the presence of the MWCNT network. Applying the proposed approach, the maximum *PCE* of DSSCs containing an optimized amount of MWCNTs (i.e., $t_{MWCNT} = 43$–48 μm) on the CE was found to be ~5.18%. This value is almost equal or slightly higher than the *PCE* of a conventional Pt-based DSSC (4.96%), suggesting that MWCNTs are suitable candidates for replacing the expensive noble Pt metal currently used in the CEs of DSSCs. The photovoltaic properties of DSSCs with MWCNT CEs can be further improved by developing a more effective ADP that would increase *FF* via the formation of a tightly bonded intranetwork among MWCNTs. By the development of a multiple-nozzle ADP system, the yield of transparent functional MWCNT thin films can be easily scaled up, thereby making possible massive production of MWCNT thin film-deposited DSSCs for practical industrial applications.

Acknowledgements

This study was supported by the National Research Foundation of Korea (NRF) funded by the Korean government (MEST) (2011-0013114). This study was also partially supported by the Global Frontier R&D Program at the Center for Multiscale Energy System funded by the

National Research Foundation under the Ministry of Education, Science and Technology, Korea (2012M3A6A 7054863).

References

Ahn, K.S., Yoo, S.J., Kang, M.S., Lee, J.W., Sung, Y.E., 2007. J. Power Sources 168, 533–536.
Cha, S.I., Koo, B.K., Seo, S.H., Lee, D.Y., 2010. J. Mater. Chem. 20, 659.
Anwar, H., George, A.E., Hill, I.G., 2013. Sol. Energy 88, 129–136.
Dürr, M., Bamedi, A., Yasuda, A., Nelles, G., 2004. Appl. Phys. Lett. 84, 3397.
Fan, B., Mei, X., Sun, K., Ouyang, J., 2008. Appl. Phys. Lett. 93, 143103.
Fang, X., Ma, T., Guan, G., Akiyama, M., 2004. J. Electroanal. Chem. 570, 257–263.
Grätzel, M., 2001. Nature 414, 338–344.
Grätzel, M., 2003. J. Photochem. Photobiol. C: Photochem. Rev. 4, 145–153.
Halme, J., Toivola, M., Tolvanen, A., Lund, P., 2006. Sol. Energy Mater. Sol. Cells 90, 872–886.
Heiniger, L.P., O'Brien, P.G., Soheilnia, N., Yang, Y., Kherani, N.P., Grätzel, M., Ozin, G.A., Tétreault, N., 2013. Adv. Mater. 25, 5734–5741.
Hsieh, C.T., Yang, B.H., Lin, J.Y., 2011. Carbon 49, 3092–3097.
Huang, S., Sun, H., Huang, X., Zhang, Q., Li, D., Luo, Y., Meng, Q., 2012. Nanoscale Res. Lett. 7, 222.
Imoto, K., Takahashi, K., Yamaguchk, T., Komura, T., Nakamura, J., Murata, K., 2003. Sol. Energy Mater. Sol. Cells 79, 459–469.
Jelle, B.P., Breivik, C., Røkenes, H.D., 2012. Sol. Energy Mater. Sol. Cells 100, 69–96.
Jo, Y., Cheon, J.Y., Yu, J., Jeong, H.Y., Han, C.H., Jun, Y., Joo, S.H., 2012. Chem. Commun. 48, 8057–8059.
Lee, W.J., Ramasamy, E., Lee, D.Y., Song, J.S., 2009. ACS Appl. Mater. Interfaces 1, 1145–1149.
Li, G.R., Wang, F., Jiang, Q.W., Gao, W.P., Shen, P.W., 2010. Nanotechnology 49, 3653–3656.
Lin, C.Y., Lin, J.Y., Lan, J.L., Wei, T.C., Wan, C.C., 2010. Electrochem. Solid-State Lett. 13, D77–D79.
Moon, Y.K., Lee, J.B., Lee, J.K., Kim, T.G., Kim, S.H., 2009. Langmuir 25, 1739–1743.
Murakami, T.N., Grätzel, M., 2008. Inorg. Chim. Acta 361, 572–580.
Nattestad, A., Ferguson, M., Kerr, R., Cheng, Y.B., Bach, U., 2008. Nanotechnology 19 (295394), 2008.
Olsen, E., Hagen, G., Lindquist, S.F., 2000. Sol. Energy Mater. Sol. Cells 63, 267–273.
O'Regan, B., Grätzel, M., 1991. Nature 353, 737–740.
Papageorgiou, N., 2004. Coord. Chem. Rev. 248, 1421–1446.
Ramasamy, E., Lee, W.J., Lee, D.Y., Song, J.S., 2008. Electrochem. Commun. 10, 1087–1089.
Siriroj, S., Pimanpang, S., Towannang, M., Maiaugree, W., Phumying, S., Jarernboon, W., Amornkitbamrung, V., 2012. Appl. Phys. Lett. 100, 243303.
Takahashi, T., Tsunoda, K., Yajima, H., Ishii, T., 2006. Jpn. J. Appl. Phys. 43, 3636–3639.
Yan, J., Uddin, M.J., Dickens, T.J., Okoli, O.I., 2013. Sol. Energy 96, 239–252.
Yoon, S., Tak, S., Kim, J., Jun, Y., Kang, K., Park, J., 2011. Build. Environ. 446, 1899–1904.